Bioactive Materials 38 (2024) 181–194

Contents lists available at ScienceDirect

Bioactive Materials

journal homepage: www.keaipublishing.com/en/journals/bioactive-materials

Mg-gallate metal-organic framework-based sprayable hydrogel for continuously regulating oxidative stress microenvironment and promoting neurovascular network reconstruction in diabetic wounds

Chenxi Lian [a], Jiawei Liu [a], Wenying Wei [a], Xiaopei Wu [a,b], Takashi Goto [c], Haiwen Li [a], Rong Tu [a,**], Honglian Dai [a,b,*]

[a] State Key Laboratory of Advanced Technology for Materials Synthesis and Processing, Wuhan University of Technology, Wuhan, 430070, China
[b] National Energy Key Laboratory for New Hydrogen-ammonia Energy Technologies, FoshanXianhu Laboratory, Foshan, 528200, China
[c] Chaozhou Branch of Chemistry and Chemical Engineering Guangdong Laboratory, Chaozhou 521000, China

ARTICLE INFO

Keywords:
Chronic diabetic wounds
Bioactive MOF
Antioxidant
Anti-inflammation
Enzymatic catalysis
Neurovascular network reconstruction

ABSTRACT

Chronic diabetic wounds are the most common complication for diabetic patients. Due to high oxidative stress levels affecting the entire healing process, treating diabetic wounds remains a challenge. Here, we present a strategy for continuously regulating oxidative stress microenvironment by the catalyst-like magnesium-gallate metal-organic framework (Mg-GA MOF) and developing sprayable hydrogel dressing with sodium alginate/chitosan quaternary ammonium salts to treat diabetic wounds. Chitosan quaternary ammonium salts with antibacterial properties can prevent bacterial infection. The continuous release of gallic acid (GA) effectively eliminates reactive oxygen species (ROS), reduces oxidative stress, and accelerates the polarization of M1-type macrophages to M2-type, shortening the transition between inflammation and proliferative phase and maintaining redox balance. Besides, magnesium ions adjuvant therapy promotes vascular regeneration and neuronal formation by activating the expression of vascular-associated genes. Sprayable hydrogel dressings with antibacterial, antioxidant, and inflammatory regulation rapidly repair diabetic wounds by promoting neurovascular network reconstruction and accelerating re-epithelialization and collagen deposition. This study confirms the feasibility of catalyst-like MOF-contained sprayable hydrogel to regulate the microenvironment continuously and provides guidance for developing the next generation of non-drug diabetes dressings.

1. Introduction

Diabetes has been ranked as one of the top 10 deadly diseases worldwide, posing a serious threat to human health [1]. Chronic diabetic wounds that are difficult to heal millions of diabetic patients, typically diabetic foot ulcers. Oxidative stress and low-grade inflammation are important features of diabetes that affect wound healing [2]. Compared with the normal wound healing process in the four overlapping stages, including hemostasis, inflammation, proliferation, and maturation, chronic diabetic wounds always prolong or stagnate in the inflammatory phase and hardly transit to the proliferative phase. The high-intensity oxidative stress environment triggered by excess free radicals, including reactive oxygen species (ROS) and reactive nitrogen species (RNS), is the key factor enhancing the inflammatory response in the early stage of injury repair and causing oxygen damage to inhibit cell behavior and tissue regeneration in the later stage [3–5]. Therefore, excess ROS/RNS scavenging is one of the effective strategies to accelerate wound repair in chronic diabetes.

Low concentrations of ROS produced by cellular metabolism are essential for physiological processes [6,7]. However, oxygen damage from excess ROS adversely affects cell viability and behavior, which delays wound healing [2]. In the early stage of damage repair, ROS enhances the expression of proinflammatory factors, such as tumor necrosis factor (TNF-α), Interleukin-1β (IL-1β), and Interleukin 6 (IL-6),

Peer review under responsibility of KeAi Communications Co., Ltd.
* Corresponding author. State Key Laboratory of Advanced Technology for Materials Synthesis and Processing, Wuhan University of Technology, Wuhan, 430070, China.
** Corresponding author.
E-mail addresses: turong@whut.edu.cn (R. Tu), daihonglian@whut.edu.cn (H. Dai).

https://doi.org/10.1016/j.bioactmat.2024.04.028
Received 27 January 2024; Received in revised form 19 April 2024; Accepted 23 April 2024

etc., amplifies the initial chronic low-grade inflammatory response, which is conducive to the M1 polarization of macrophages [3]. Active M1 macrophages enhance ROS accumulation, forming a vicious cycle and inducing the risk of bacterial infection. On the other hand, poor skin cells behavior under oxidative stress, including endothelial cells, fibroblasts, and epidermal cells, directly suppresses the transition from inflammation to proliferation. In the proliferation and maturation stage, the formation of blood vessels or neural networks is crucial in skin repair. However, excess ROS can activate matrix metalloproteinases, leading to extracellular matrix degradation and weakening adhesion, migration, and cell signaling of vascular and neuron-associated cells, thereby limiting the regeneration rate and function of blood vessels or neural networks [8]. Therefore, it is necessary to rapidly reduce oxidative stress levels in the early stage and maintain redox balance until the wound is repaired.

Although excess ROS can be defended by endogenous antioxidant enzymes (superoxide dismutase (SOD), catalase (CAT), and NADPH, etc.) and exogenous antioxidants (Vitamin E, vitamin C, etc.) [9]. The balance between antioxidants and ROS in the diabetic microenvironment is disrupted due to the decreased function of antioxidant enzymes [10]. To solve this phenomenon, inorganic nanozymes represented by ferric oxide [11], cerium dioxide [12,13], manganese oxide [14–16], etc., are used to regulate ROS levels due to their enzyme-like catalytic function. Compared with the potential biotoxicity and undesirable degradability of inorganic nanoenzymes, natural polyphenols are considered to be good biocompatible antioxidants and anti-inflammatory agents due to the free radical scavenging properties of phenolic hydroxyl groups [17]. Phthalic polyphenols such as tannins (TA) [18], epigallocatechin gallate (EGCG) [19], and gallic acid (GA) [20] are well-known as anti-oxidative reagents to develop biomaterials. However, the stability of phenolic hydroxyl groups makes it difficult for these molecules to achieve a sustainable antioxidant process when used alone.

Incorporating small molecule polyphenols into the biological metal-organic framework (bio-MOF) is a novel and effective way to improve catalytic efficiency and bioavailability. Introducting the antioxidant small molecules directly as ligands for MOF and releasing them through the *in vivo* degradation avoids additional toxic side effects caused by the

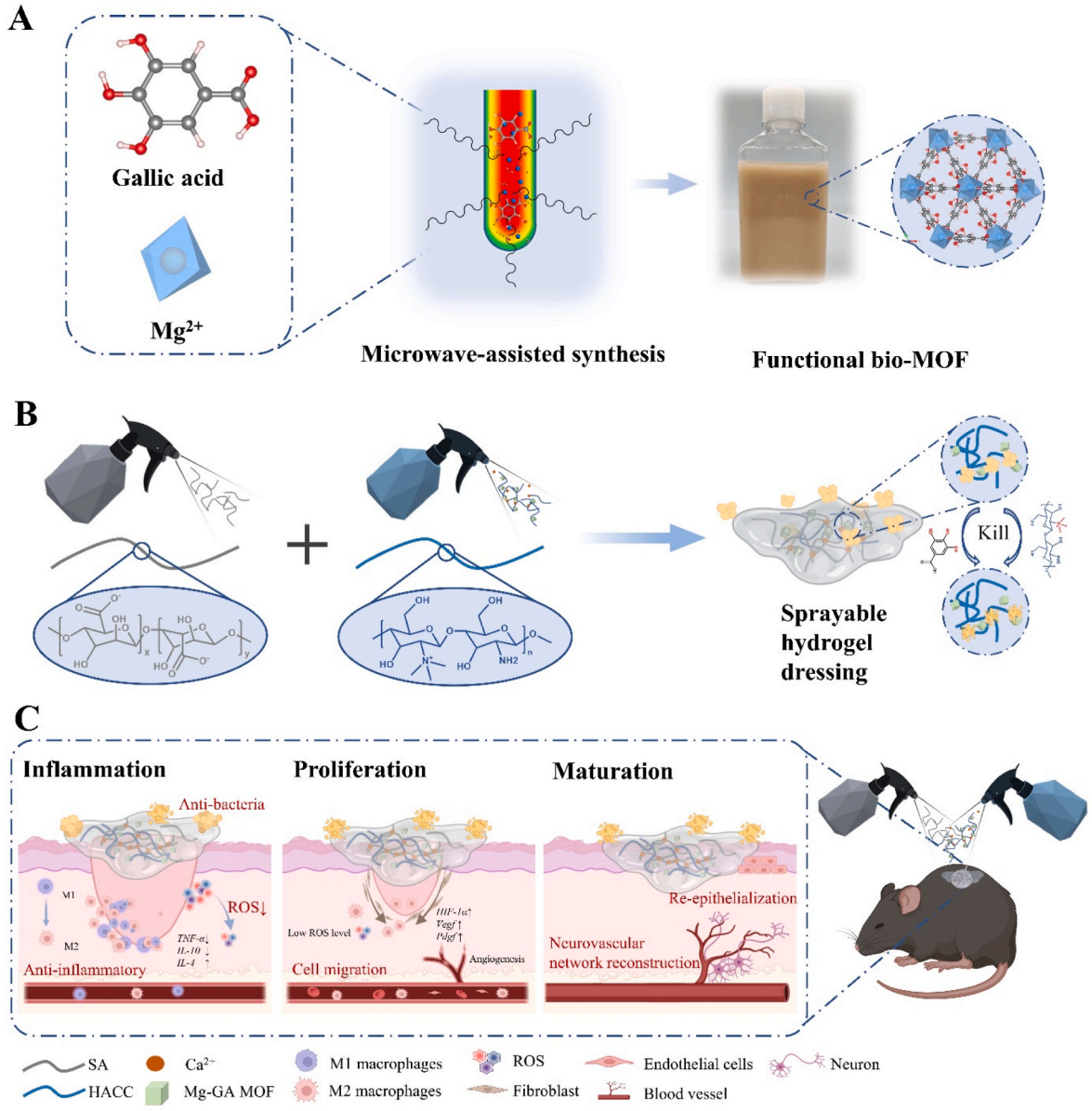

Scheme 1. Schematic Illustrations of (A) Synthesis of Mg-GA MOF, (B) Synthesis of sprayable hydrogel dressing containing Mg-GA MOF, and (C) Mechanism for promoting chronic diabetes wound repair.

degradation of nonactive ligands during drug delivery via MOF pore size loading [21–23]. At the same time, bioactive metal ions are used as central ions to confer more biological effects on bio-MOF. Representative, bioactive ions (such as Mg^{2+}, Si^{4+}, and Cu^{2+}) have been greatly studied in vascular or nerve regeneration [24–27]. Using gallic acid-based bio-MOF as an antioxidant platform to maintain low levels of oxidative stress while enhancing vascular and neurological function by bioactive ions adjuvant therapy is a good new strategy for the treatment of chronic diabetic wounds.

Herein, we propose a new antibacterial sprayable hydrogel dressing (Gel/MOF) containing magnesium-gallate metal-organic framework (Mg-GA MOF) with enzyme-catalytic function to achieve chronic diabetic wound repair. (Scheme 1). Mg-GA MOF with stable performance and uniform morphology can be obtained using microwave-assisted synthesis technology. In the early stage of wound repair, the GA released by Mg-GA MOF rapidly achieves ROS-scavenging, reducing oxidative stress levels and anti-inflammatory effectively. Mg-GA MOF continuously releases GA and Mg^{2+} during biodegradation to maintain redox balance and enhance vascular and nerve regeneration in the late stages of wound repair. The sprayable hydrogel is formed by fast crosslinking between atomized sodium alginate (SA) and high-concentration calcium ion solution. Moreover, chitosan quaternary ammonium salt (HACC), an effective antibacterial component, was added to the sprayable hydrogel to realize the inhibition and elimination of bacteria, which is also a major factor affecting the recovery of chronic diabetic wounds. This Gel/MOF significantly regulates the microenvironment and promotes chronic diabetic wound repair by enhancing neurovascular network reconstruction, collagen deposition, and re-epithelialization.

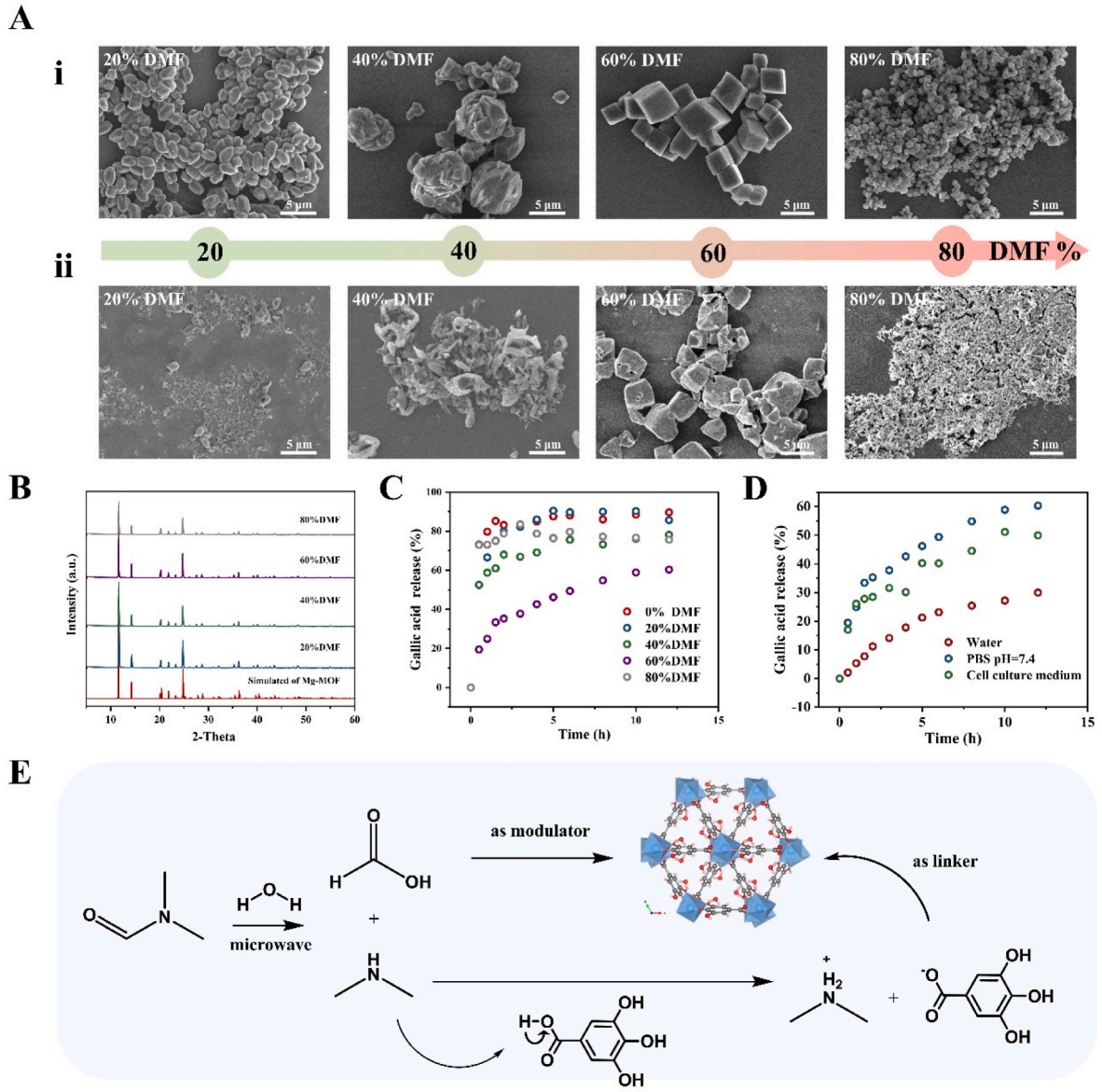

Fig. 1. Mg-GA MOF with controlled morphology releases gallic acid continuously. A) Representative SEM micrographs of i) Mg-GA MOF morphology prepared under different DMF/aqueous solvent systems and ii) the morphology of Mg-GA MOF after degradation in phosphate buffer (PBS, pH 7.4). B) X-ray diffraction (XRD) patterns of Mg-GA MOFs. C) The release profiles of GA from Mg-GA MOF prepared under different DMF/water systems in PBS (pH 7.4). D) The release behavior of Mg-GA MOFs synthesized at 60 % DMF/water system in deionized water, PBS (pH 7.4), and cell culture medium. E) Mechanism of DMF regulating crystal morphology.

2. Results and discussion

2.1. Mg-GA MOF releases gallic acid continuously

The magnesium-gallate metal-organic framework (Mg-GA MOF) was prepared using microwave-assisted synthesis technology, which was further optimized based on the reported synthesis method [28]. N, N-dimethylformamide (DMF)/water (v/v) binary solvent system and microwave-assisted hydrothermal method were employed to shorten the synthesis time and obtain a monodisperse morphology. The results of scanning electron microscopy (SEM) showed that the Mg-GA MOF prepared with N, N-dimethylformamide (DMF)/water (v/v) solvent system were uniform (~5 μm) and monodisperse compared with the traditional hydrothermal synthesis method and the pure water system (Fig. 1A-i and Figs. S1A–B). With the increase of DMF content, the morphology of Mg-GA MOF changed. Mg-GA MOFs were double cones under the 20 % DMF/water system, which gradually changed into cubes as the concentration of DMF increased to 60 % and finally changed into spheres under the 80 % DMF/water solvent system. Further increasing the DMF content would make it difficult to form a stable Mg-GA MOF, obtaining only a few products. The corresponding energy-dispersive X-ray spectroscopy (EDS) of the Mg-GA MOF prepared under the 60 % DMF/water shows uniform distribution of elemental (Fig. S2). The X-ray diffraction (XRD) results showed that the Mg-GA MOF prepared under the DMF/water system still had the main sharp characteristic peaks and resembled the simulated patterns of Mg-GA MOF (Fig. 1B). It means that changing the solution system does not change the structure of the Mg-GA MOF. However, the diffraction intensity of the strongest peak decreased with the DMF concentration increased to 80 %. The thermogravimetric analysis results showed that the Mg-GA MOF prepared under the DMF/water system was $Mg(H_2gal)\cdot 2H_2O$ (Figs. S3A–D) [28]. The results showed that the uniform and monodisperse Mg-GA MOFs could be obtained quickly using the improved method, and the presence of DMF had little effect on crystallinity.

Compared with the traditional hydrothermal reaction that requires a long time (12–24 h) at high temperatures (>120 °C), microwave-assisted synthesis transfers uniform and high-density energy to the reaction system in a relatively short time. A large number of products can be obtained after the reaction at 90 °C for 30 min. The presence of DMF enhances the polarity of the solvent so that the transition state during the reaction process is easy to be solvated, the free enthalpy is reduced, and the reaction speed is accelerated. Meanwhile, DMF is hydrolyzed to produce formic acid and dimethylamine as regulators and deprotonation, respectively [29]. On the one hand, the binding energy of formate-Mg^{2+} is similar to that of gallate-Mg^{2+} (the binding energy of them are ~ -370 mol/kJ in the ideal state, verified by materials studio simulations), formate can coordinate with Mg^{2+} in crystal synthesis to stabilize the structure. On the other hand, dimethylamine deprotonates gallic acid, accelerating the binding of ligands to central ions (Fig. 1E). It realized energy-saving and stable large-scale production. Moreover, DMF could regulate the morphology of the product and enhance the stability of the monodisperse particles in addition to enhancing dispersion as a solvent.

To investigate the effects of different crystal morphologies on the degradation of Mg-GA MOF and the release of gallic acid (GA), Mg-GA MOFs were dispersed in phosphate-buffered saline (PBS, pH 7.4) and shaken at 37 °C. The morphology of Mg-GA MOFs after the release of GA for 24 h was shown in Fig. 1A-ii and the release profiles of GA were presented in Fig. 1C. Among them, the morphology of Mg-GA MOF synthesized under the 60 % DMF/water system was still relatively complete, and cubic morphology was still clearly visible. The Mg-GA MOF prepared under the 20 or 40 % DMF/water system had a few block structures. However, the Mg-GA MOF prepared under the 80 % DMF/water system had only fragments and could not be distinguished as individual particles. Meanwhile, the higher the DMF content of the reaction system (not higher than 60 %), the slower the release rate of GA from Mg-GA MOF during the first 5 h. However, the release rate of GA from Mg-GA MOF increased abruptly when DMF content increased to 80 %. The results showed that the content of DMF in the solvent system affected the stability of Mg-GA MOF. Mg-GA MOF prepared under the 60 % DMF/water solvent system had the highest stability, and that prepared in the 80 % DMF/water had a higher degradation rate than other systems due to the relatively low crystallinity and extreme instability in the solution. Moreover, the GA release rate of Mg-GA MOF prepared under 60 % DMF/aqueous system is only 66 % after 12 h, which is 30 % lower than that of the traditional hydrothermal method (Fig. S1C).

Further, to observe the release behavior of Mg-GA MOFs in different solutions, the Mg-GA MOFs synthesized at 60 % DMF/water solvent system were preferred and dispersed in deionized water, PBS (pH 7.4), and cell culture medium. Mg-GA MOF released ~30 % GA in water after 12 h but more than 50 % in PBS and medium for only 10 h (Fig. 1D). The release profiles showed that the GA release rate in water was significantly lower than in PBS and medium. Due to the hydrophilicity of gallic acid and the affinity between the phosphate ions and Mg^{2+}, Mg-GA MOF in PBS and medium degraded relatively faster than in water, which has a certain affinity for degradable Mg-GA MOFs in organisms and will effectively release GA [30].

Bio-MOF materials have been widely studied and applied, but their instability in water is a key factor limiting their development. In general, stable MOF structures have broader application potential. Optimizing the synthesis method of Mg-GA MOF can improve the stability in water which would help to improve the catalytic performance.

2.2. Enzyme-catalytic function of Mg-GA MOF to scavenge ROS

For chronic diabetic wounds, excess ROS are the most critical mediators affecting the rate of wound healing. To determine whether the Mg-GA MOF has the ability to mimic enzymatic catalysis, a series of ROS-scavenging experiments were performed, including the typical representatives such as superoxide anions ($O_2\cdot^-$), hydrogen peroxide (H_2O_2), hydroxyl radicals (·OH), and 1,1-diphenyl-2-picryl-hydrazyl radical (DPPH·). Since the catalytic reduction of ROS by Mg-GA MOF is mainly related to ligand GA and the surface-active sites of MOF, in this section, we compare Mg-GA MOF with GA and the common antioxidant ascorbic acid (vitamin C), an effective antioxidant in the body, to evaluate the ability of Mg-GA MOFs to scavenge various free radicals.

Superoxide dismutase (SOD) is an enzyme that catalyzes $O_2\cdot^-$ to H_2O_2 and O_2 by dismutation in eukaryotes. The SOD-like activity of Mg-GA MOF was determined by detecting the inhibition of nitroblue tetrazolium (NBT) reduction. The results showed the low absorption peak at 560 nm for Mg-GA MOF groups, indicating the SOD-like ability of Mg-GA MOF. Meanwhile, with the increased concentration, the SOD-like ability of Mg-GA MOF obviously improved (Fig. 2B and Fig. S4A). However, when the dose of Mg-GA MOF was increased to 5 mg/mL, 50 % of $O_2\cdot^-$ could not be removed. For superoxide radicals, the scavenging ability of Mg-GA MOF and AA has no significant gap. The ability of Mg-GA MOFs to scavenge O_2^- is mainly due to the release of ligands GA. Ascorbic acid (AA) is a dibasic acid, AA^- is more stable than AA^{2-} and AA, and AA^- reacts faster with O_2^- than AA directly, therefore, AA scavenging superoxide radicals is mainly due to AA dehydrogenation to produce ascorbate (AA^-) [31]. The O–H bond dissociation energy (BDE) is one of the indicators to evaluate the scavenging of ROS by polyphenolic antioxidants (hydrogen atom transfer mechanism) [32,33]. The lower the BDE, the stronger the antioxidant effect. However, the BDE of O–H in GA is much lower than the first-order dissociation energy of AA, so the efficiency of GA in scavenging superoxide radicals is much faster than that of AA.

H_2O_2 is one of the common reactive oxygen molecules in the body, mainly produced by SOD enzyme catalytic production and degraded by catalase (CAT). The CAT-like capacity of Mg-GA MOF was confirmed by using titanium sulfate colorimetry. Fig. S4B shows that the absorption at

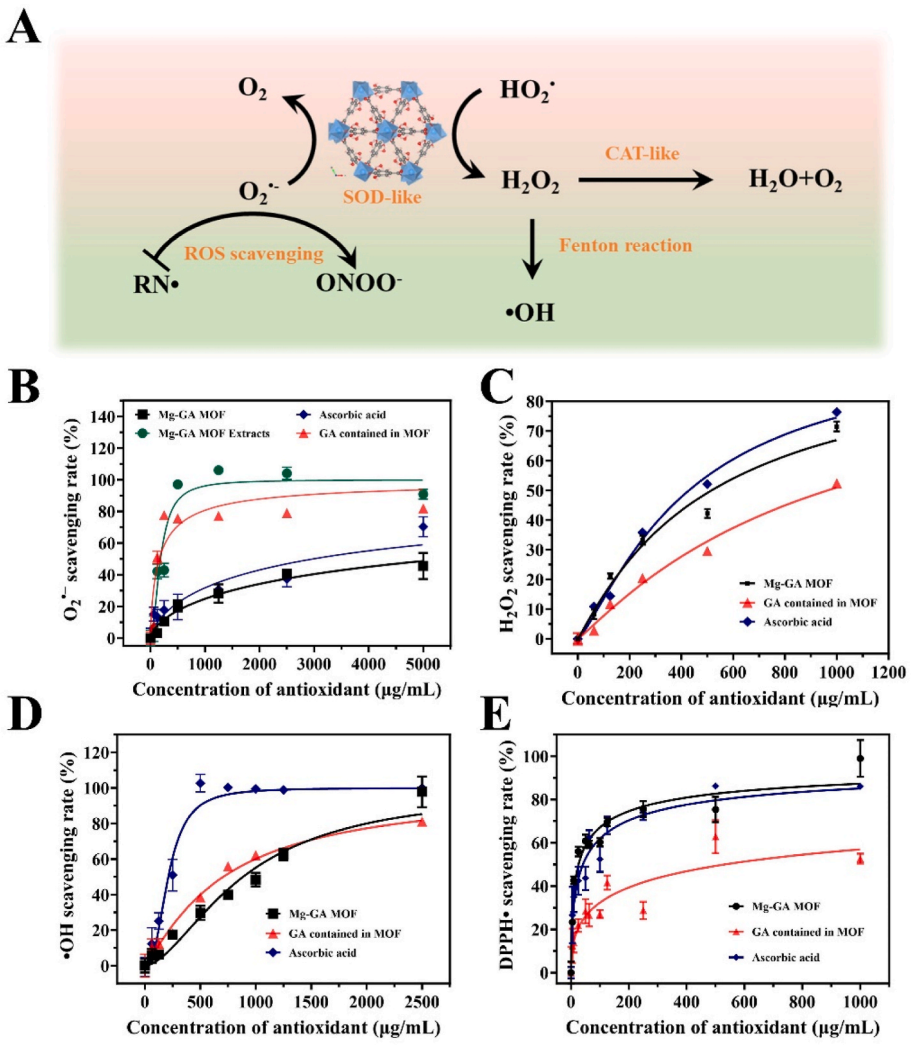

Fig. 2. Mg-GA MOF has the enzyme-catalytic function to scavenge ROS. A) Mechanism of ROS and RNS scavenging from Mg-GA MOF. ROS-scavenging ratio of Mg-GA MOF including B) $O_2^{\bullet-}$, C) H_2O_2, and D) •OH. E) DPPH•-scavenging ratio of Mg-GA MOF.

405 nm was significantly reduced after incubating with Mg-GA MOF. The H_2O_2-scavenging rate increased significantly with the increase of Mg-GA MOF concentration (Fig. 2C). The result showed that 42.9 % of H_2O_2 was eliminated after being incubated with Mg-GA MOF ($C_{Mg\text{-}GA\ MOF}$ = 500 μg/mL). Mg-GA MOF has the CAT-like catalytic ability to scavenge H_2O_2 and is not significantly different from AA. But the reaction rate is greater than the same amount of GA contained in Mg-GA MOF, which may be due to the adsorption of H_2O_2 by Mg-GA MOF to accelerate the reaction rate, or related to its surface active site. Notably, the dose-dependence for the CAT-like ability of Mg-GA MOF was less than that of SOD-like activity.

The •OH are the most oxidative endogenous free radicals. Highly active •OH can directly cause irreversible oxygen damage to lipids, proteins, and DNA [34]. Significantly, •OH is produced through the iron-dependent Fenton reaction, which attacks all biomolecules at a diffusion-controlled rate and often initiates a chain reaction, but any specific antioxidant enzyme can not scavenge it [35]. The •OH -scavenging ability of Mg-GA MOF was evaluated by salicylic acid indicator. As Figure S4C and Fig. 2D showed, the absorption peak at 510 nm in the Mg-GA MOF group decreased significantly compared with the control group. And the higher the concentration of Mg-GA MOF, the more the decrease. The half-inhibitory concentration (IC50) of Mg-GA MOF for ·OH was approximately 885 μg/mL, and the scavenging effect was similar to that of GA. The phenolic hydroxyl group on GA can provide electrons to scavenge •OH or block the Fenton reaction [36]. However, it is significantly lower than ascorbic acid. It is because the addition reaction between the C3 position of AA and •OH is barrier-free, and the final addition product is also stable [37]. So AA can quickly scavenge •OH. Moreover, the •OH-scavenging efficiency is also concentration-dependent with Mg-GA MOF, and its concentration dependence is between SOD-like and CAT-like.

Reactive nitrogen radicals (RNS) are considered to be special ROS, nitrogen-containing radicals produced by the reaction of nitric oxide (NO) with active substances in the body [38]. RNS is closely related to the inflammatory response because of the high expression of inducible nitric oxide synthase (iNOS) in M1-type macrophages, resulting in NO accumulation [39]. DPPH· is a very stable nitrogen-centered free radical widely used as the RNS-scavenging model. After Mg-GA MOF incubating with DPPH· solution at 37 °C for 30 min, the decrease in the absorption peak at 517 nm was measured by UV–Vis spectrophotometer. The IC50 of Mg-GA MOF for DPPH· was 25.84 μg/mL. In comparison, traditional antioxidant ascorbic acid required 41.02 μg/mL to achieve the effect of scavenging half of the DPPH, both of which were better than that of GA· (Figure S4D and Fig. 2E). The results demonstrated Mg-GA MOF has a scavenging effect on DPPH free radicals due to the single-electron/proton transfer of the phenolic hydroxyl group in gallic acid, which was better than traditional antioxidants ascorbic acid.

In conclusion, Mg-GA MOF with enzyme-catalytic ability could

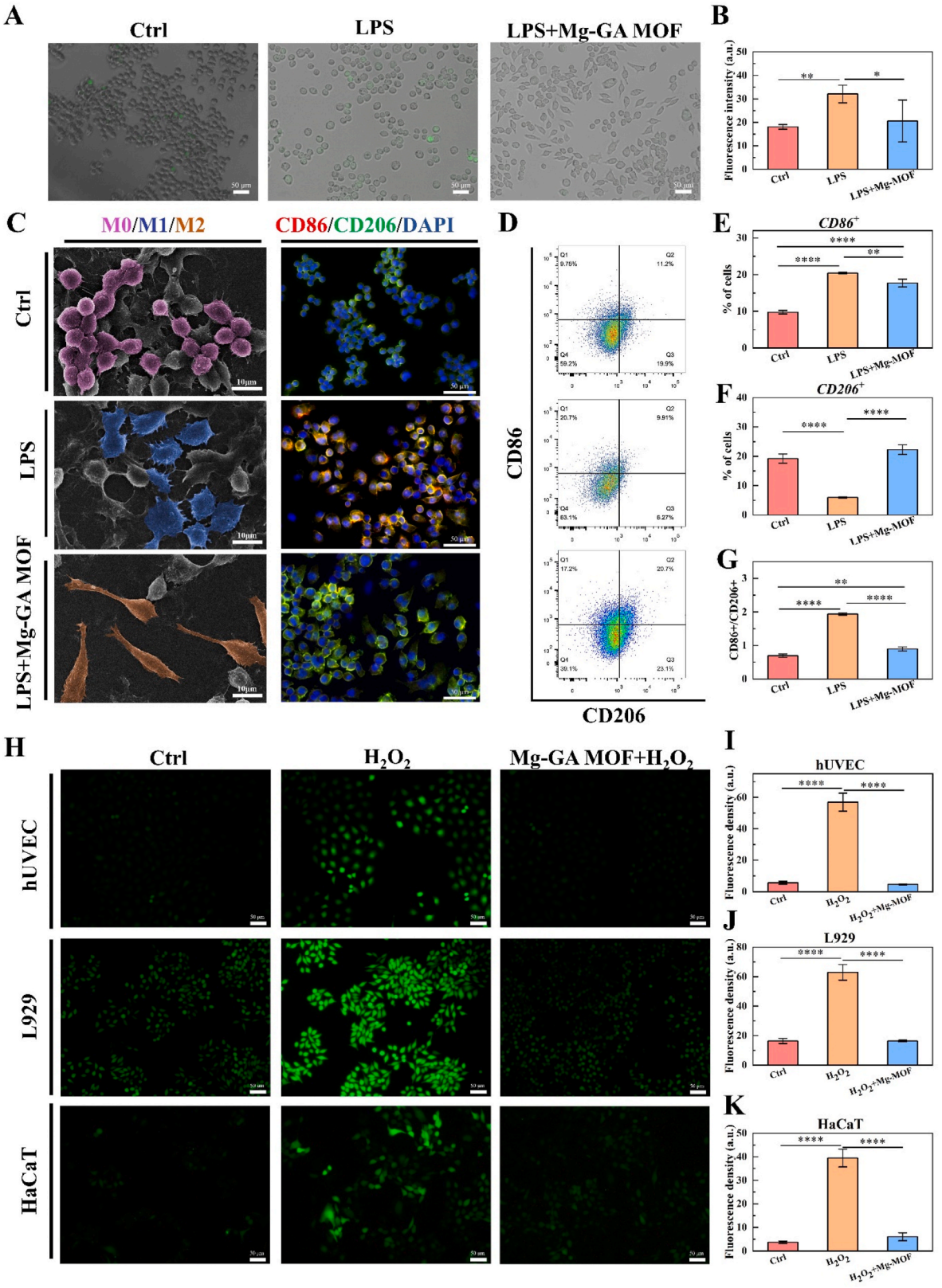

Fig. 3. Mg-GA MOF could be anti-inflammatory and antioxidant *in vitro*. A) Brightfield and ROS fluorescence merge images and B) intracellular ROS fluorescence intensity of RAW 264.7. Scale bars: 50 μm. C) Representative SEM images and immunofluorescence images for $CD86^+$ and $CD206^+$ of RAW 264.7 after LPS and Mg-GA MOF treatment (purple for M0 type; blue cells for M1 type; orange cells for M2 type). D) The results of RAW 264.7 flow cytometry and E-G) semi-quantitative analysis of $CD86^+$ and $CD206^+$. H–K) Mg-GA MOF protects hUVEC, L929, and HaCaT cells from oxygen damage and intracellular ROS fluorescence intensity analysis. Scale bars: 50 μm.

scavenge various reactive oxygen radicals to maintain redox homeostasis. It is worth noting that the activities of SOD-like and CAT-like for Mg-GA MOF have potential advantages in $O_2^{\cdot-}$-scavenging and H_2O_2-scavenging for cascade catalytic reactions. Moreover, the dose-dependence of CAT-like for MG-GA MOF is less than that of SOD-like and OH-scavenging, effectively avoiding the accumulation of H_2O_2 caused by SOD-like catalysis and the formation of ·OH by additional Fenton reaction. In addition, the efficient RNS-scavenging performance with low-dose Mg-GA MOF breaks the accumulation of peroxynitrite anion (ONOO-), an RNS with stronger oxidation than NO and produced by further reactions of NO and $O_2^{\cdot-}$. It avoids nitrosation stress, as this RNS can easily cause DNA fragmentation and lipid peroxidation.

2.3. In vitro anti-inflammatory and antioxidant abilities of Mg-GA MOF

The inflammatory response plays a key role in the repair of chronic diabetic wounds [40,41]. In the process of diabetic wound repair, the key to rapid wound repair is to reduce the level of oxidative stress and shorten the inflammatory phase in the early stage. Firstly, to verify the *in vitro* anti-inflammatory activity of Mg-GA MOF, we induced RAW264.7 cells with lipopolysaccharides (LPS) to establish an inflammation model. Before that, it is necessary to investigate whether the material is toxic to RAW264.7 cells. Mg-GA MOF was non-cytotoxic, and the cell viability increased on the 3 days of culture, and the cell morphology changed from stereospherical to spindle-shaped (Figs. S5A–B). LPS triggers macrophage inflammation response while increasing the ROS level [42,43]. To investigate whether Mg-GA MOF can reduce oxidative stress in inflammatory environments, the reactive oxygen species fluorescent probe 2,7- dichlorodi-hydrofluorescein diacetate (DCFH-DA) was used to detect intracellular ROS content. Fig. 3A and B showed that while flat pancake-shaped cells (M1 type) in the LPS group with strong green fluorescence, the control group had less ROS content, and the LPS + Mg-GA MOF treatment group transformed into long spindle-shaped cells (M2 type) and ROS^+ green fluorescence intensity was significantly reduced in them. It suggests that LPS stimulates the RAW264.7 inflammatory response while producing a large amount of intracellular ROS and increasing the level of oxidative stress. Mg-GA MOF regulates the polarization of macrophages by reducing intracellular ROS levels and improving inflammatory mediators.

SEM images of RAW 264.7 after LPS and Mg-GA MOF treatment again verified macrophage polarization (Fig. 3C). Compared with the untreated group, the LPS-induced cells changed from stereo spherical-shaped (purple cells, M0 type) to flat pancake-shaped (blue cells, M1 type), and then changed to long spindle-shaped (orange cells, M2 type) after Mg-GA MOF treatment. Furthermore, M1 and M2 macrophages respectively labeled with $CD86^+$ and $CD206^+$, respectively, were analyzed for phenotypic transformation by immunofluorescence staining and flow cytometry. Fig. 3C-Gand Fig. S6 shows the immunofluorescence images and the results of flow cytometry and semi-quantitative analysis. The content of $CD86^+$ cells increased significantly after LPS stimulation, indicating that RAW264.7 cells differentiated towards the M1 type. Subsequently, the content of $CD206^+$ cells increased significantly after Mg-GA MOF incubation, indicating that RAW264.7 cells were polarized from M1 to M2, transforming proinflammatory to anti-inflammatory state. At the same time, the value of $CD86^+/CD206^+$ of cells was significantly lower than that in control and LPS groups after LPS+Mg-GA MOF treatment. The results showed that Mg-GA MOF could promote the polarization of M1 to M2 in RAW264.7 cells and had *in vitro* anti-inflammatory activity.

Furthermore, the related proteins of RAW264.7 cells were detected by western blotting (WB). As Fig. S7 showed, the result verified that the expression of M1 macrophage-related protein (TNF-α, IL-6, iNOS) was increased after LPS stimulation, and the expression of M2 macrophage-associated protein (ARG-1, IL-10, TGF-β) was increased in the group induced by the addition of Mg-GA MOF. It is similar to the results of previous experiments and further validates the ability of Mg-GA MOF to induce M1 polarization to M2 *in Vitro*.

Under oxidative stress, ROS inhibited cell survival and proliferation, resulting in slow tissue regeneration [44]. The continuous maintenance of low levels of ROS and the protection of skin-related cells from oxygen damage during tissue regeneration are the guarantees for the function of regenerating skin. To evaluate whether Mg-GA MOF could protect cells from oxygen damage, we used different cells, including vascular endothelial cells (hUVEC), mouse fibroblast (L929), and human keratinocytes (HaCaT). Figs. S8A and B demonstrate Mg-GA MOFs below 50 μg/mL are almost no cytotoxicity to hUVEC cells and L929 cells and even promote the proliferation of HaCaT cells. Morever, the cells survival were significantly improved by pro-protecting of Mg-GA MOF before exposure to excess ROS, compared with the untreated group (H_2O_2 treatment only). Considering the tolerance of different cells to different concentrations of material extracts, 50 μg/mL Mg-GA MOF was determined as the material intervention group for related experiments. To further verify the protective effect of Mg-GA MOF on different skin cells, we used reactive oxygen fluorescent probes DCFH-DA to detect intracellular ROS levels. High-intensity green fluorescence was observed in group cells directly exposed to H_2O_2 without pro-protection, confirming that intracellular ROS levels increased significantly after oxygen damage ($p < 0.0001$). However, the fluorescence intensity in the group pre-cultured of Mg-GA MOF was comparable to the control group, indicating that the cells were not damaged by oxygen (Fig. 3H–K). Therefore, Mg-GA MOF exhibited excellent performance in resisting H_2O_2 attacks and avoiding cellular oxygen damage, attributed to the antioxidation of gallic acid [20].

For chronic diabetic wounds, persistent oxidative stress and the impaired immune environment are the keys to hinder wound healing. Mg-GA MOF can protect the immune cells in oxidative environment, accelerating the transition from M1 to M2. In addition to early immune regulation, the rapid reaction with high-intensity ROS in the inflammatory environment could decrease the level of oxidative stress. The prolonged degradation of Mg-GA MOF also realized long-term maintenance of oxidative stress balance, which directly relates to the efficiency of damage repair in the later stage and functional reconstruction of damage repair in the later stage.

2.4. In vitro endothelial cell migration and the tubule formation enhanced by Mg-GA MOF

Angiogenesis plays a key role in tissue regeneration, depending on the migration of vascular endothelial cells and vascular network formation [45,46]. To confirm the promotion effect of Mg-GA MOF on angiogenesis, a scratch assay was first performed to investigate the migration effect of hUVEC cells. Fig. 4A showed that the hUVEC cells migration range of the 50 μg/mL Mg-GA MOF-treated group was significantly larger than that of the untreated group. After 24 h of treatment, the mobility rate of the Mg-GA MOF group reached 71.45 %, while that of the control group was only 58 % (Fig. 4C). This result insinuated that Mg-GA MOF could promote endothelial cell migration, attributed to the Mg^{2+} released by Mg-GA MOF [47].

Furthermore, the tubule formation assay was performed on hUVEC cells *in vitro* to evaluate the tubulogenic effect of Mg-GA MOF. As shown in Fig. 4B, after 3 h of incubation, only a few cells tended to form tubes in the control group, but the tubules in the Mg-GA MOF group were already observed clearly. After another 3 h, the tubule formation effect of the control group was only slightly enhanced, which was still significantly lower than that of the Mg-GA MOF group. It was observed that hUVECs cultured with Mg-GA MOF could significantly improve tubule formation at both treatment times compared to the untreated control group. Semi-quantitative statistical statistics further confirmed this result. After 3 h of incubation, the number of branches and the length of tubes in the Mg-GA MOF group were 4-fold higher than that of the control group. After 6 h of treatment, although increasing in the control group, it was far less effective than the tube-forming effect in the Mg-GA MOF group (Fig. 4D

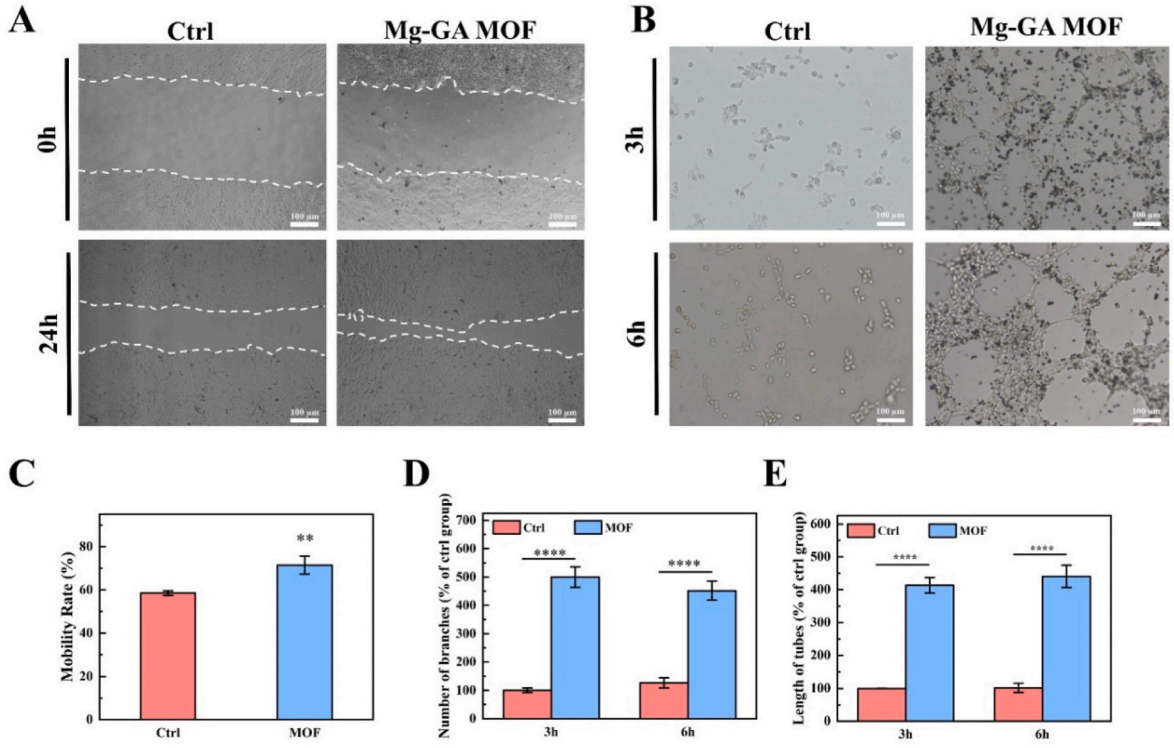

Fig. 4. Angiogenesis effect of Mg-GA MOF. Representative images of the effect of Mg-GA MOF on hUVEC cell migration A) and cell mobility rate C) were evaluated by scratch assay from 0 to 24 h. B) Mg-GA MOF promotes *in vitro* tube formation of endothelial cells. Representative brightfield images after 3 h and 6 h treatment and semi-quantitative statistical of D) the number of branches and F) the length of the tubes. Scale bars: 100 μm.

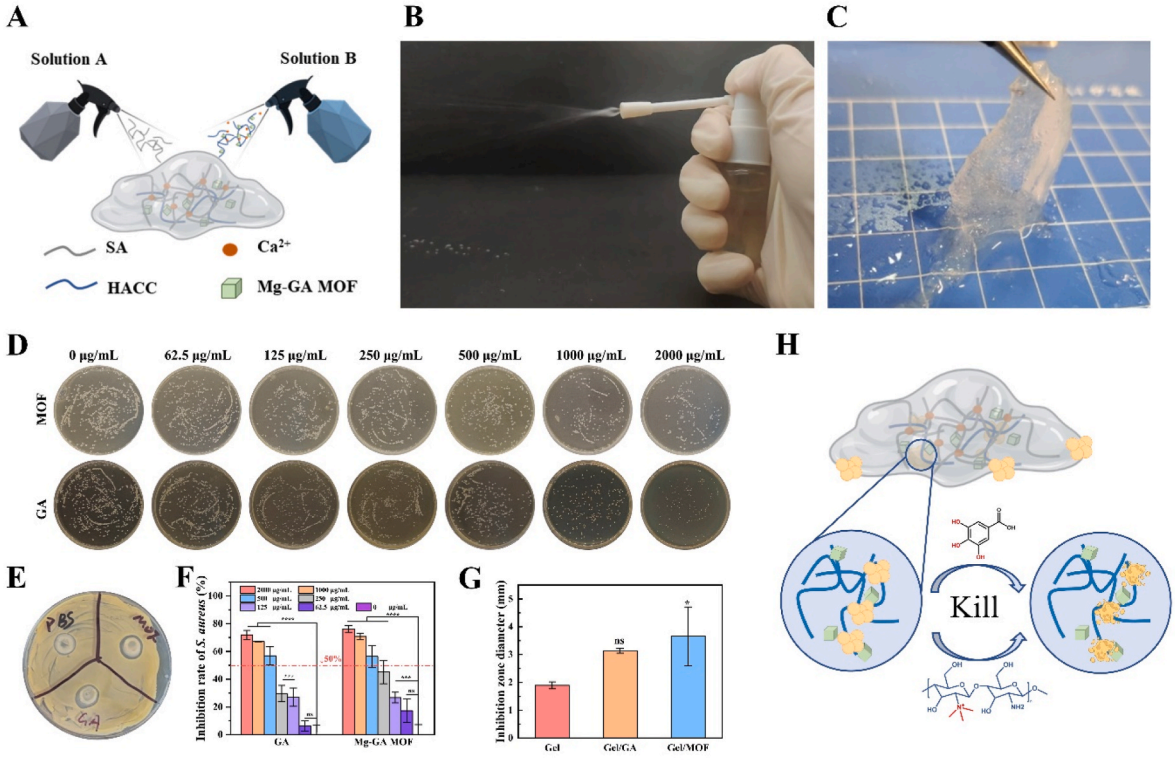

Fig. 5. Sprayable hydrogel dressings containing Mg-GA MOF are effective in bacterial inhibition. A) Schematic diagram of the preparation of sprayable hydrogel dressing. B) Spraying of the Gel/MOF hydrogel dressing. C) Hydrogel dressing molding image. Representative image D) of Mg-GA MOF and GA inhibition against *S. aureus* and the inhibition rate F) were determined by colony forming units (CFU). E and G) The zone of inhibition test was evaluated against the *S. aureus* effect of Gel, Gel/GA, and Gel/MOF hydrogel dressing (PBS for Gel without GA and MOF, MOF for Gel with MOF, GA for Gel with GA). H) Diagram of the mechanism of Gel/MOF antibacterial effect.

and E).

In summary, the results demonstrated that Mg-GA MOF could significantly promote endothelial cell migration and enhance tubule formation *in vivo*, which has a potential and critical role in revascularization.

2.5. Mg-GA MOF-based sprayable antibacterial gel dressing

To efficiently deliver Mg-GA MOF in diabetic wounds, we synthesized a sprayable hydrogel dressing with Mg-GA MOF (Gel/MOF). The sol-gel transformation of the hydrogel dressing was achieved by mutual spraying of A and B solutions, where A solution is an aqueous solution of sodium alginate (SA), and B is a calcium ion solution of chitosan-quaternary ammonium salt (HACC) containing Mg-GA MOF. The atomized SA and calcium ion solution were rapidly crosslinked in about tens of seconds (Fig. 5A–C).

To explore the antibacterial property of the hydrogel dressings, we first evaluated the antimicrobial performance of Mg-GA MOF and GA by colony forming unit (CFU) assay. Gallic acid, the ligand of Mg-GA MOF, has a unique antibacterial efficacy and has been widely studied as an antimicrobial agent [20,48]. After gram-positive *Staphylococcus aureus* (*S. aureus*, BNCC 186335) was incubated with Mg-GA MOFs for 24 h, the CFU assay and semi-quantification result showed that with the concentration of Mg-GA MOF or GA increasing, the inhibition effect for *S. aureus* was enhanced, and the half inhibit concentration (IC 50) of Mg-GA MOF against *S. aureus* was lower than GA (Fig. 5D and F). Mg-GA MOF and GA have similar effects on the inhibition of *Escherichia coli* (*E. coli*, BNCC336902) (Fig. S9). It is worth noting that the antibacterial effect of gallic acid and its derivatives is not obvious, and the minimum inhibitory concentration of most of them is $>$ 2000 μg/mL [49,50]. It means Mg-GA MOF could inhibit and eliminate bacteria, but this property highly depended on concentration. It is the general property of natural polyphenols and the disadvantage of Mg-GA MOF alone as an antibacterial agent.

As cationic antibacterial agents, quaternary ammonium salts can adsorb to the surface of negatively charged bacteria and change the membrane permeability of bacteria to achieve bactericidal purpose [51,52]. Quaternary ammonium salts modified chitosan introduced to Gel/MOF can improve the antibacterial sensitivity of the hydrogel dressing. The zone of inhibition test was evaluated against the *S. aureus* effect of gel dressing. Fig. 5E and G showed the zone of inhibition and the bacteriostatic circle diameters after incubation of Gel/MOF, Gel/GA, and Gel (hydrogel dressing without MOF) for 24 h. Gel, Gel/GA, and Gel/MOF could both inhibit the growth of *S. aureus*. Gel/MOF exhibited a stronger inhibitory effect on the growth of *S. aureus* with an inhibition circle diameter of 3.66 ± 1.05 mm, which was significant improved to that of Gel and Gel/GA (inhibition circle diameter was 1.89 ± 0.12 mm and 3.14 ± 0.08 mm). In the control group without the addition of chitosan quaternary ammonium salt, no obvious antibacterial effect was observed even with the addition of GA or MOF (Figure S10 A-B). For *E. coli*, the Gel contained with chitosan quaternary ammonium salt did not have a good inhibitory effect, mainly due to the poor antibacterial ability of chitosan quaternary ammonium salt against gram-negative bacteria [53]. It is worth noting that most wound infections are mainly caused by *S. aureus*, and this complex hydrogel still has a certain therapeutic effect on wound infections.

In summary, the poor antimicrobial effect of gallic acid itself and its need to be released in solution may be the main reason for the lack of obvious antibacterial effect. The continuous release of gallic acid from Mg-GA MOF in the hydrogel dressing after the adsorption of bacteria by quaternary ammonium salts. The synergistic effect of the gallic acid and quaternary ammonium salts achieves a better antibacterial effect. Therefore, Gel/MOF has a potential advantage in inhibiting bacteria proliferation in wounds and preventing bacterial growth in the long term.

2.6. Sprayable hydrogel dressing accelerated diabetic wound healing in vivo

To verify whether sprayable hydrogel dressing accelerates diabetic wound repair, we evaluated Gel/MOF on full-thickness skin defect with a diameter of 6 mm in db/db diabetic mice (Fig. 6A). As Fig. 6B–D showed, there was no significant gap between the groups in the first three days after surgery. On the fourth day, the wound area of Gel/MOF had been reduced to 57.95 ± 4.45 %. It was significantly smaller than that of the control group and the Gel group. After the 8 days, the Gel-treated groups decreased wound area compared with the control group but still had a significant gap with Gel/MOF group. Notably, the healing rate of the Gel/MOF group accelerated significantly from eight days after surgery. It may have transformed from the inflammatory to the proliferative phase, which benefited from the positive regulation of macrophages and the reduction of ROS levels by the released GA. On the other hand, GA and Mg^{2+} improved the wound microenvironment and guaranteed subsequent wound healing. On day 12, the wound area in the Gel/MOF group had been reduced to 2.86 ± 1.18 %, compared with only 7.12 ± 0.60 % in the Gel group and 9.75 ± 1.58 % in the control group on day 16.

Histological section staining of regenerated skin tissue on day 16 was performed to evaluate the effect of Gel/MOF on diabetic wound healing histologically. The H&E staining results were showed in Fig. 6E–F. Although the thickness of the regenerated epidermis had not differed much from the control group after treatment with Gel and Gel/MOF, the control group could clearly identify the location of the wound. Meanwhile, compared with the basic wound healing in the Gel group, the wound in the Gel/MOF group was completely healed and almost identical to the surrounding skin tissue, and more blood vessels, hair follicles, and sebaceous glands were visible (the arrows in the figure indicated). Meanwhile, the control group was mainly germ tissue. It demonstrated that Mg-GA MOF could accelerate wound reconstruction by promoting the regeneration of the skin tissue appendages.

The epidermis is a complex multilayer squamous epithelium, and the formation of functional keratin is the key to epidermal differentiation. During the terminal differentiation of epidermal keratinocytes from the basal keratocytes to the spinous keratocytes, proliferation-specific cytokeratin 14 (K14) is gradually replaced by differentiation-specific cytokeratin 10 (K10) [54]. To evaluate the effect on re-epithelialization, we specifically marked using K14 and K10 to stain tissue sections on day 16. Compared with the Gel group, the total amount of cytokeratin increased significantly in the group treated with Gel/MOF, and the content in the epidermis of K10 and K14 increased from 80.76 % to 90.36 % and from 59.85 % to 62.27 %, respectively (Fig. 6J and K). It is worth noting that the control group had excessive secretion of K10 under the low K14 level, accompanied by the not-obvious stratum granulosum boundary and thickening of the stratum granulosum and stratum spinosum (Fig. 6H). The results suggested abnormal cytokeratin secretion and the possibility of hyperkeratinization in the control group. Besides epidermal proliferative basal cells, K14 is also expressed in sebaceous glands and the outer root sheath of hair follicles [55,56]. Fig. S11 showed a significantly strong fluorescence and increase in K14 level at the hair follicles compared to the control group, which strongly confirms the H&E results.

The collagen deposition of regenerated tissue is detected by Masson staining (Fig. 6E and G). It observed the Gel and Gel/MOF groups exhibited significantly more collagen deposition than the control group, and the Gel/MOF group was ~1.18-fold higher than the Gel group. The type of collagen deposition was further analyzed by picrosirius red staining (Fig. 6I and L). On day 16, the collagen in the control group was showed yellow-green, and it was changed to orange-yellow and bright red after Gel and Gel/MOF treatment. The Gel/MOF group had a higher collagen I/III ratio than the control and Gel groups. Type I and type III collagen play an important role in skin repair, mainly expressing type III collagen in the early stage and then gradually replaced with type I

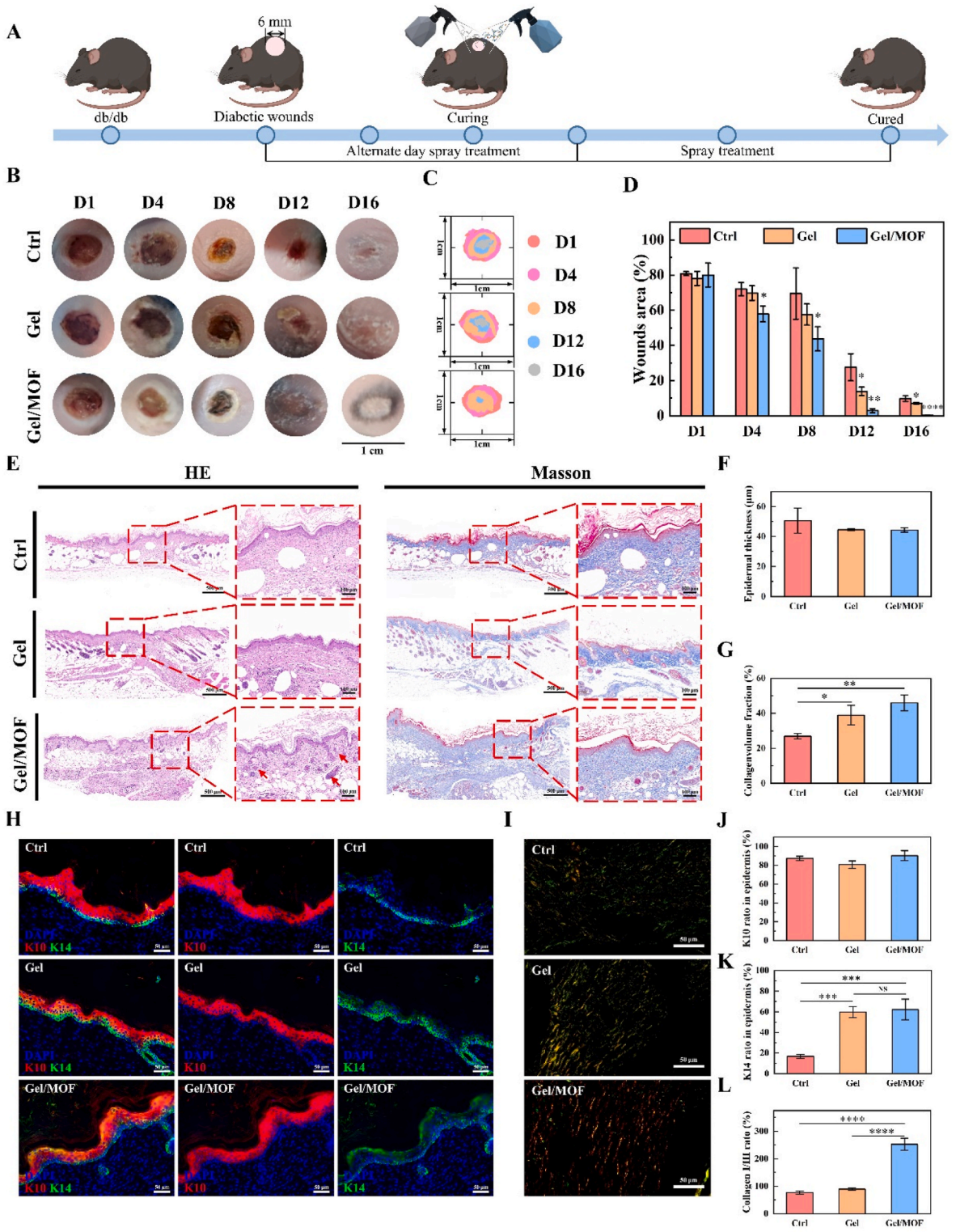

Fig. 6. Sprayable hydrogel dressing accelerated diabetic wound healing *in vivo*. A) Schematic illustration of the sprayable hydrogel dressing treatment in the db/db mice wound model. B) Representative photograph of db/db mice wounds, C) wound trace superimposed images, and D) wound area with or without Gel and Gel/MOF treatment on 1, 4, 8, 12, and 16 days after surgery. E) H&E and Masson staining of regenerating skin on day 16. Scale bars: 500 μm and 100 μm. Semi-quantitative analysis of F) the epithelial thickness of regenerated tissue in H&E staining and G) the total collagen deposition in Masson staining. H) Cytokeratin 10 (K10, red) and Cytokeratin 14 (K14, green) immunofluorescent staining and J-K) semi-quantitative analysis in the regenerated epithelium on day 16. Scale bars: 50 μm. I) Distribution of types I and III collagen in regenerated skin on day 16 by Sirius red staining. Scale bars: 50 μm. L) Quantification of collagen I/III ratio.

collagen. Type I collagen has a very strong promoting effect on the adhesion and migration of keratinocytes [57]. It indicated Gel/MOF promotes collagen deposition and regulates type I and III collagen expression to promote wound healing.

2.7. Gel/MOF inhibited oxidative stress and regulated the inflammatory response in diabetic wound

A series of experiments were performed to verify that Gel/MOF could accelerate the inflammation-proliferative transition *in vivo* by reducing oxidative stress and regulating the inflammatory response. First, Gel and Gel/MOF treatment significantly reduced the total intracellular ROS content (Fig. 7A and B). On day 8, the density of ROS^+ cells was extremely significantly reduced after Gel and Gel/MOF treatment compared to the control group. Particularly, the ROS^+ cell density of Gel/MOF was significantly lower than that of the Gel group ($p < 0.01$), demonstrating that the presence of MOF increased ROS-scavenging and greatly relieved the microenvironment of oxidative stress in diabetic wounds.

Second, RT-qPCR was used to detect inflammation-related genes in regenerated skin tissues on day 8. In the early stage of inflammation, M1 macrophages secrete proinflammatory factors represented to activate the inflammatory response. In the late stage of inflammation and the early stage of proliferation, the M1 macrophages transform into the M2 [58–60]. Tumor necrosis factor (*TNF-α*), Interleukin-10 (*IL-10*), and Interleukin-4 (*IL-4*) were selected as representative proinflammatory or anti-inflammatory factors to evaluate the inflammatory regulation of Gel/MOF in the early repair of diabetic wounds. The results showed that although the *TNF-α* gene expression in the Gel/MOF group was not significantly reduced, the expression of anti-inflammatory factors *IL-10* and *IL-4* in the Gel/MOF group was significantly higher than that in the control and Gel groups (Fig. 7C–E).

Further, the inflammation-associated proteins were extracted from the Gel and Gel/MOF group and then detected using cytokine protein arrays (Fig. 7F and G). The proinflammatory cytokines Interleukin-1α (IL-1α), Interleukin-16 (IL-16), C–C motif chemokine ligand 3 (CCL3), C-X-C motif chemokine ligand 2 (CXCL2), and C-X-C motif chemokine ligand 3 (CXCL3) were reduced in the gel/MOF group, while the anti-inflammatory factor IL-1ra increased. The results demonstrated that adding MOF to gel dressings enhanced the polarization of M1 macrophages to M2 type and actively regulated the inflammatory microenvironment for promoting wound healing.

2.8. Gel/MOF accelerated neurovascular network reconstruction

The oxidative stress microenvironment directly affects vascularity and neurogenesis [61,62]. To investigate whether inhibited oxidative stress by MOF could positively affect vascular regeneration during the proliferative phase, we detected the regenerated tissue for vascular-associated genes (Fig. 8A–C). On day 8, the hypoxia-inducible factor 1-α (HIF-1α) expression increased significantly after Gel/MOF treatment. At the same time, the expression of vascular endothelial

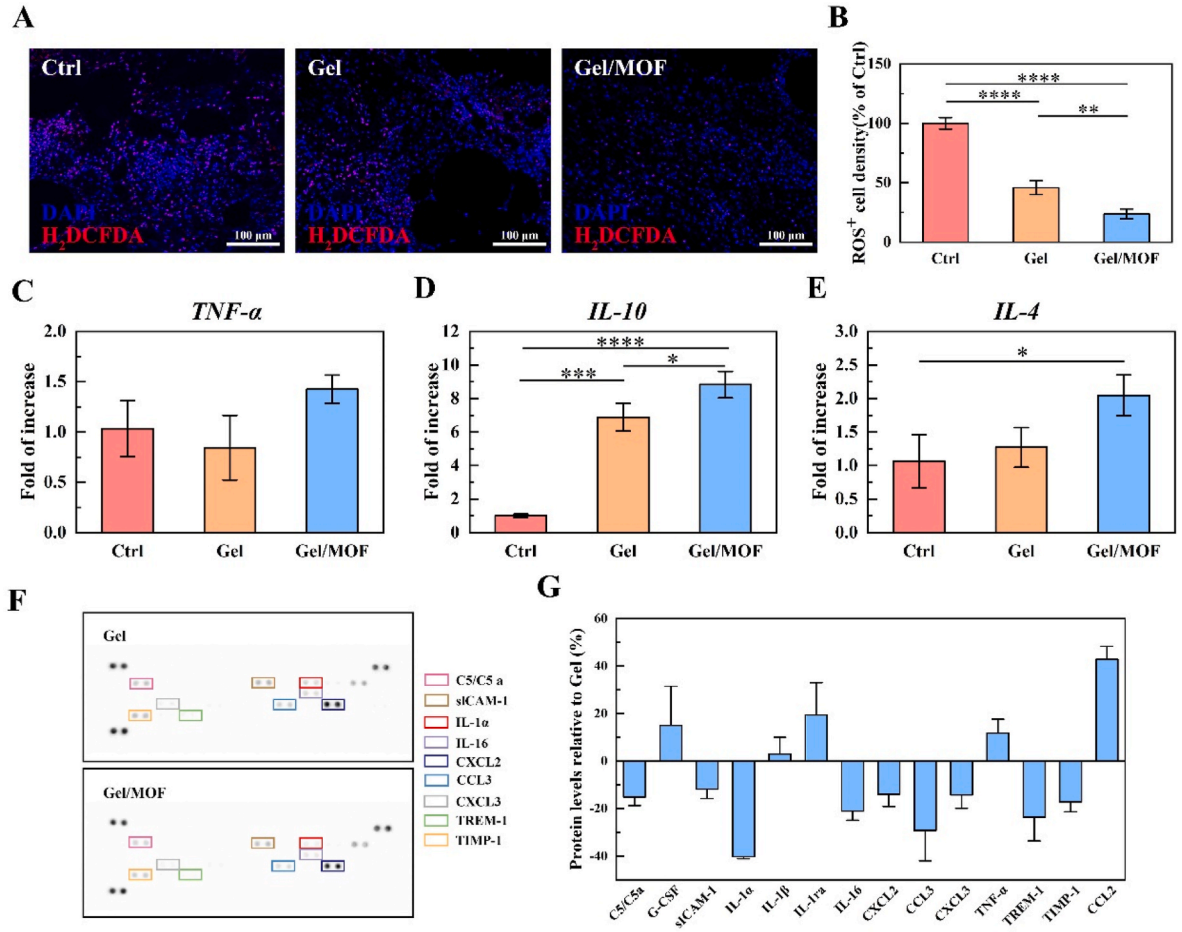

Fig. 7. Sprayable hydrogel dressing containing Mg-GA MOF regulated inflammatory cytokine expression and inhibited oxidative stress in diabetic wounds. A) Immunofluorescence staining of H_2DCFDA (red) and B) ROS^+ cell density on day 8. Scale bars: 50 μm. Relative gene expression of C) tumor necrosis factor (*TNF-α*), D) interleukin-10 (*IL-10*), E) and interleukin-4 (*IL-4*) in the diabetic wounds on day 8. F) and G) Cytokine array and analysis of the inflammation-related factor levels after Gel and Gel/MOF treatment on 8 days.

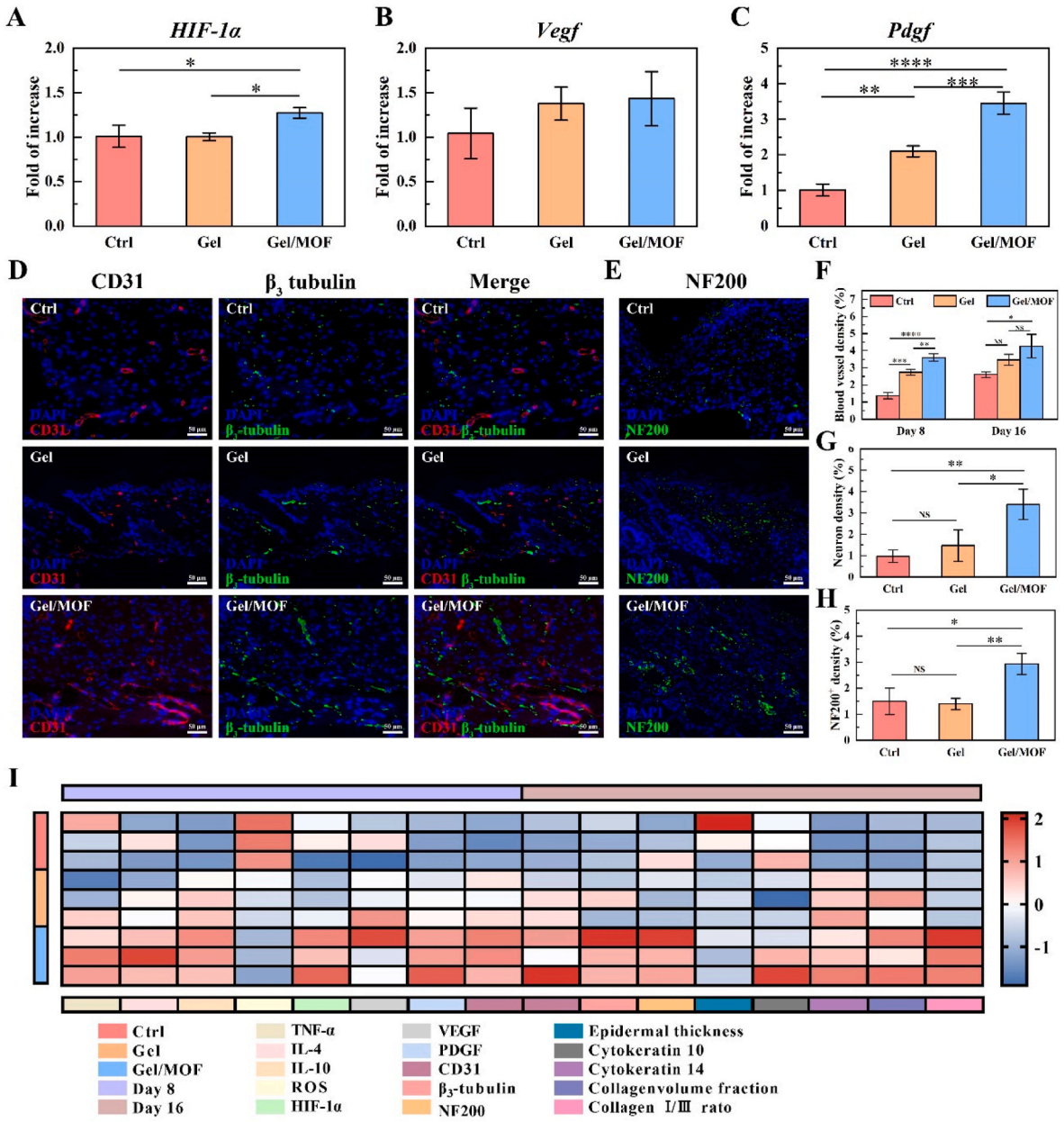

Fig. 8. Sprayable hydrogel dressing containing Mg-GA MOF accelerated neurovascular network reconstruction. A-C) Relative gene expression of hypoxia-inducible factor 1-α (*HIF-1α*), vascular endothelial growth factor (*Vegf*), and platelet-derived growth factor (*Pdgf*) in the diabetic wounds on day 16. D) Immunofluorescence double staining of CD31 (red) and β_3-tubulin (green) on day 16. Scale bars: 50 μm. E) Immunofluorescence staining of NF200 on day 16. Scale bars: 50 μm. F) Blood vessel and G) neuron density on day 16 after treatment with or without Gel and Gel/MOF. H) $NF200^+$ density in immunofluorescence staining. I) Heatmap analysis of multiple indicators of diabetic regenerated wounds.

growth factor (*Vegf*) and platelet-derived growth factor (*Pdgf*) genes increased, and the relative expression of *Pdgf* in the Gel/MOF group was significantly higher than that in control ($p < 0.0001$) and Gel group ($p < 0.001$). The expression of *HIF-1α* after Gel/MOF treatment was similar to that of *TNF-α*. The high metabolic activity of inflammatory cells and vasoconstriction caused by inflammatory factors formed a hypoxic environment and activated the expression of *HIF-1α*, which mainly targets *Vegf* gene [[63,64]. Meanwhile, Mg^{2+} released by Mg-GA MOF could upregulate the expression of *Vegf* and *Pdgf* [65]. Under dual action, the proliferation and migration of vascular endothelial cells and the formation of new blood vessels are promoted. It is the key factor in quickly ending the inflammatory phase and entering the proliferative phase.

Further, CD31, β_3-tubulin, and NF200 were used to mark the vascular and neuronal of the regenerated skin tissue at 8 and 16 days (Fig. 8D–H and Fig. S12). On day 8, the control group showed a few $CD31^+$. In contrast, Gel and Gel/MOF showed a large number of $CD31^+$. The semi-quantitative results showed that the blood vessel density of the control group ($p < 0.0001$) and Gel ($p < 0.01$) group was significantly lower than that of the Gel/MOF group. On day 16, $CD31^+$ increased compared to day 8, but the blood vessel density of the control group was still significantly lower than that in the Gel/MOF group ($p < 0.05$). At the same time, the Gel/MOF group showed a large continuous strip-shaped β_3-$tubulin^+$ coloring, most of which were around $CD31^+$, while the control group showed only faint β_3-$tubulin^+$ and fewer in the Gel group. The nerve density of the Gel/MOF group was significantly higher than that in the control group ($p < 0.01$) and the Gel group ($p < 0.05$). It means that the nascent neural network existed in the regenerated skin

after Gel/MOF treatment. NF200 immunofluorescence staining once again confirmed this result, which had similar results to β_3-tubulin$^+$. The NF200 fluorescence intensity in the Gel/MOF group was significant higher than in the control and Gel groups on day 16. It is worth noting that most of the new nerves and blood vessels exist in the form of companions, suggesting a better repair effect and stronger functional potential for the skin after Gel/MOF treatment.

The comprehensive analysis of multiple indicators of skin regeneration is in Fig. 8I. With inflammation positively regulated, ROS levels decreased, and angiogenesis-associated cytokine *HIF-1α*, *Vegf*, and *Pdgf* were secreted after Gel and Gel/MOF treatment. GA and Mg^{2+} released continuously by Mg-GA MOF maintained low ROS levels in the later stage of inflammation, effectively protected the activated vascular-related genes, and rapidly formed neovascularization. When blood vessels grew rapidly during proliferation, relatively complete neurons were also regenerated. It may be attributable to the fact that *Pdgf* activated neural-related activities as neurotrophic factors at the same time [66]. The concomitant regeneration of blood vessels and nerves is the foundation for skin remodeling, followed by collagen deposition and re-epithelialization to achieve the repair of chronic diabetic wounds.

3. Conclusion

Mg-GA MOF was successfully prepared and used as a microenvironment regulator for treating chronic diabetic wounds by loading into a sprayable hydrogel dressing with antibacterial properties. Compared with traditional synthesis methods, the preparation of Mg-GA was achieved in large-scale production with single dispersion and adjustable morphology by microwave-assisted synthesis. Mg-GA MOF with enzyme-like catalytic activity can quickly remove ROS and maintain redox balance by degrading to release GA, effectively regulating the microenvironment of chronic diabetic wounds. In the later stages of wound repair, bioactive magnesium-ions adjuvant therapy enhances neurovascular network reconstruction, while antibacterial hydrogel dressing prevents bacterial infections. This simple and convenient sprayable hydrogel dressing offers a new strategy for chronic diabetic wounds without drug treatment.

4. Experimental section/methods

Detailed protocols are presented in supporting information.

Ethics approval and consent to participate

All experimental procedures were conducted in accordance with institutional guidelines for the care and use of laboratory animals and protocols, which were approved by the Animal Ethics Committee of Wuhan University of Technology (Protocol No. 2022-021). Cell source: HACAT BNCC339817, L929 BNCC100314, HUVEC BNCC342438, RAW264.7 BNCC354753.

CRediT authorship contribution statement

Chenxi Lian: Writing – review & editing, Writing – original draft, Investigation, Data curation, Conceptualization. **Jiawei Liu:** Writing – review & editing, Investigation, Conceptualization. **Wenying Wei:** Writing – review & editing, Investigation, Validation. **Xiaopei Wu:** Writing – review & editing, Funding acquisition. **Takashi Goto:** Writing – review & editing. **Haiwen Li:** Writing – review & editing. **Rong Tu:** Writing – review & editing. **Honglian Dai:** Conceptualization, Writing – review & editing, Supervision, Project administration, Funding acquisition.

Declaration of competing interest

The authors declare no conflict of interest.

Acknowledgements

This work was supported by grants from the National Natural Science Foundation of China (52372272, 32201109, 32360234), the National Key Research and Development Program of China (2022YFB4601402), the Guangdong Basic and Applied Basic Research Foundation (2022B1515120052, 2021A1515110557), the Key Basic Research Program of Shenzhen (JCYJ20200109150218836), and the Self-innovation Research Funding Project of Hanjiang Laboratory (HJL202202A002). The authors thank the help of Tong Qiu, Qinghua Hou and Ran Yu of the Wuhan University of Technology, Wuhan 430070, China.

Appendix A. Supplementary data

Supplementary data to this article can be found online at https://doi.org/10.1016/j.bioactmat.2024.04.028.

References

[1] X. Lin, Y. Xu, X. Pan, J. Xu, Y. Ding, X. Sun, X. Song, Y. Ren, P.F. Shan, Global, regional, and national burden and trend of diabetes in 195 countries and territories: an analysis from 1990 to 2025, Sci. Rep. 10 (1) (2020) 14790.
[2] J. Moura, P. Madureira, E.C. Leal, A.C. Fonseca, E. Carvalho, Immune aging in diabetes and its implications in wound healing, Clin. Immunol. 200 (2019) 43–54.
[3] E. Naik, V.M. Dixit, Mitochondrial reactive oxygen species drive proinflammatory cytokine production, J. Exp. Med. 208 (3) (2011) 417–420.
[4] M. Mittal, M.R. Siddiqui, K. Tran, S.P. Reddy, A.B. Malik, Reactive oxygen species in inflammation and tissue injury, Antioxidants Redox Signal. 20 (7) (2014) 1126–1167.
[5] R. Moseley, J.E. Stewart, P. Stephens, R.J. Waddington, D.W. Thomas, Extracellular matrix metabolites as potential biomarkers of disease activity in wound fluid: lessons learned from other inflammatory diseases? Br. J. Dermatol. 150 (3) (2015) 401–413.
[6] B. Castro, M. Citterico, S. Kimura, D.M. Stevens, M. Wrzaczek, G. Coaker, Stress-induced reactive oxygen species compartmentalization, perception and signalling, Nat. Plants 7 (4) (2021) 403–412.
[7] D. Trachootham, J. Alexandre, P. Huang, Targeting cancer cells by ROS-mediated mechanisms: a radical therapeutic approach? Nat. Rev. Drug Discov. 8 (7) (2009) 579–591.
[8] M.A. Incalza, R. D'Oria, A. Natalicchio, S. Perrini, L. Laviola, F. Giorgino, Oxidative stress and reactive oxygen species in endothelial dysfunction associated with cardiovascular and metabolic diseases, Vasc. Pharmacol. 100 (2018) 1–19.
[9] A.M. Pisoschi, A. Pop, F. Iordache, L. Stanca, G. Predoi, A.I. Serban, Oxidative stress mitigation by antioxidants - an overview on their chemistry and influences on health status, Eur. J. Med. Chem. 209 (2021) 112891.
[10] Y. Xiong, X. Chu, T. Yu, S. Knoedler, A. Schroeter, L. Lu, K. Zha, Z. Lin, D. Jiang, Y. Rinkevich, A.C. Panayi, B. Mi, G. Liu, Y. Zhao, Reactive oxygen species-scavenging nanosystems in the treatment of diabetic wounds, Adv. Healthcare Mater. (2023) e2300779.
[11] F. Yu, Y. Huang, A.J. Cole, V.C. Yang, The artificial peroxidase activity of magnetic iron oxide nanoparticles and its application to glucose detection, Biomaterials 30 (27) (2009) 4716–4722.
[12] T. Wang, Y. Li, E.J. Cornel, C. Li, J. Du, Combined antioxidant–antibiotic treatment for effectively healing infected diabetic wounds based on polymer vesicles, ACS Nano 15 (5) (2021) 9027–9038.
[13] J. Kim, G. Hong, L. Mazaleuskaya, J.C. Hsu, D.N. Rosario-Berrios, T. Grosser, P. F. Cho-Park, D.P. Cormode, Ultrasmall antioxidant cerium oxide nanoparticles for regulation of acute inflammation, ACS Appl. Mater. Interfaces 13 (51) (2021) 60852–60864.
[14] X. Jiang, P. Gray, M. Patel, J. Zheng, J.J. Yin, Crossover between anti- and pro-oxidant activities of different manganese oxide nanoparticles and their biological implications, J. Mater. Chem. B 8 (6) (2020) 1191–1201.
[15] X.L. Luo, J.J. Xu, W. Zhao, H.Y. Chen, A novel glucose ENFET based on the special reactivity of MnO2 nanoparticles, Biosens. Bioelectron. 19 (10) (2004) 1295–1300.
[16] S. Wang, H. Zheng, L. Zhou, F. Cheng, Z. Liu, H. Zhang, L. Wang, Q. Zhang, Nanoenzyme-reinforced injectable hydrogel for healing diabetic wounds infected with multidrug resistant bacteria, Nano Lett. 20 (7) (2020) 5149–5158.
[17] X. Zhang, Z. Li, P. Yang, G. Duan, X. Liu, Z. Gu, Y. Li, Polyphenol scaffolds in tissue engineering, Mater. Horiz. 8 (1) (2021) 145–167.
[18] İ. Gülçin, Z. Huyut, M. Elmastaş, H.Y. Aboul-Enein, Radical scavenging and antioxidant activity of tannic acid, Arab. J. Chem. 3 (1) (2010) 43–53.
[19] Y. Zhong, C.M. Ma, F. Shahidi, Antioxidant and antiviral activities of lipophilic epigallocatechin gallate (EGCG) derivatives, J. Funct.Foods 4 (1) (2012) 87–93.
[20] B. Badhani, N. Sharma, R. Kakkar, Gallic acid: a versatile antioxidant with promising therapeutic and industrial applications, RSC Adv. 5 (35) (2015) 27540–27557.
[21] Y. Li, Y. Miao, L. Yang, Y. Zhao, K. Wu, Z. Lu, Z. Hu, J. Guo, Recent advances in the development and antimicrobial applications of metal-phenolic networks, Adv. Sci. 9 (27) (2022) e2202684.

[22] H. Geng, Q.Z. Zhong, J. Li, Z. Lin, J. Cui, F. Caruso, J. Hao, Metal ion-directed functional metal-phenolic materials, Chem. Rev. 122 (13) (2022) 11432–11473.
[23] A.C. McKinlay, R.E. Morris, P. Horcajada, G. Férey, R. Gref, P. Couvreur, C. Serre, BioMOFs: metal-organic frameworks for biological and medical applications, Angew. Chem. Int. Ed. 49 (36) (2010) 6260–6266.
[24] Y. Xia, X. Jing, X. Wu, P. Zhuang, X. Guo, H. Dai, 3D-printed dual-ion chronological release functional platform reconstructs neuro-vascularization network for critical-sized bone defect regeneration, Chem. Eng. J. 465 (2023).
[25] P. Zhuang, Y. Yao, X. Su, Y. Zhao, K. Liu, X. Wu, H. Dai, Vascularization and neuralization of bioactive calcium magnesium phosphate/hydrogels for wound healing, Compos. B Eng. 242 (2022).
[26] S. Xiao, J. Wei, S. Jin, X. Xia, L. Yuan, Q. Zou, Y. Zuo, J. Li, Y. Li, A multifunctional coating strategy for promotion of immunomodulatory and osteo/angio-genic activity, Adv. Funct. Mater. 33 (4) (2022).
[27] N. Alasvand, A. Behnamghader, P.B. Milan, S. Simorgh, A. Mobasheri, M. Mozafari, Tissue-engineered small-diameter vascular grafts containing novel copper-doped bioactive glass biomaterials to promote angiogenic activity and endothelial regeneration, Mater. Today Biol. 20 (2023) 100647.
[28] L. Cooper, T. Hidalgo, M. Gorman, T. Lozano-Fernandez, R. Simon-Vazquez, C. Olivier, N. Guillou, C. Serre, C. Martineau, F. Taulelle, D. Damasceno-Borges, G. Maurin, A. Gonzalez-Fernandez, P. Horcajada, T. Devic, A biocompatible porous Mg-gallate metal-organic framework as an antioxidant carrier, Chem. Commun. 51 (27) (2015) 5848–5851.
[29] O.M. Yaghi, M.J. Kalmutzki, C.S. Diercks, Introduction to Reticular Chemistry: Metal-Organic Frameworks and Covalent Organic Frameworks, John Wiley & Sons, 2019.
[30] A. Sharma, A. Kumar, C. Li, P. Panwar Hazari, S.D. Mahajan, R. Aalinkeel, R. K. Sharma, M.T. Swihart, A cannabidiol-loaded Mg-gallate metal-organic framework-based potential therapeutic for glioblastomas, J. Mater. Chem. B 9 (10) (2021) 2505–2514.
[31] Y.-J. Tu, D. Njus, H.B. Schlegel, A theoretical study of ascorbic acid oxidation andHOO/O2−radical scavenging, Org. Biomol. Chem. 15 (20) (2017) 4417–4431.
[32] Thavasi Velmurugan, Peng Lai, Ryan Leong, Anthony Bettens Phillip, Investigation of the influence of hydroxy groups on the radical scavenging ability of polyphenols, J. Phys. Chem. 110 (14) (2006) 4918–4923.
[33] C. Papuc, G.V. Goran, C.N. Predescu, V. Nicorescu, G. Stefan, Plant polyphenols as antioxidant and antibacterial agents for shelf-life extension of meat and meat products: classification, structures, sources, and action mechanisms, Compr. Rev. Food Sci. Food Saf. 16 (6) (2017) 1243–1268.
[34] M. Dizdaroglu, P. Jaruga, Mechanisms of free radical-induced damage to DNA, Free Radic. Res. 46 (4) (2012) 382–419.
[35] M.S. Lord, J.F. Berret, S. Singh, A. Vinu, A.S. Karakoti, Redox active cerium oxide nanoparticles: current status and burning issues, Small 17 (51) (2021) e2102342.
[36] M. Spiegel, K. Kapusta, W. Kolodziejczyk, J. Saloni, B. Zbikowska, G.A. Hill, Z. Sroka, Antioxidant activity of selected phenolic acids-ferric reducing antioxidant power assay and QSAR analysis of the structural features, Molecules 25 (13) (2020).
[37] P. Li, Z. Shen, W. Wang, Z. Ma, S. Bi, H. Sun, Y. Bu, The capture of H and ȮH radicals by vitamin C and implications for the new source for the formation of the anion free radical, Phys. Chem. Chem. Phys. 12 (20) (2010).
[38] S. Di Meo, T.T. Reed, P. Venditti, V.M. Victor, Role of ROS and RNS sources in physiological and pathological conditions, Oxid. Med. Cell. Longev. 2016 (2016) 1245049.
[39] J. Muri, M. Kopf, Redox regulation of immunometabolism, Nat. Rev. Immunol. 21 (6) (2021) 363–381.
[40] Y. Liang, J. He, B. Guo, Functional hydrogels as wound dressing to enhance wound healing, ACS Nano 15 (8) (2021) 12687–12722.
[41] M. Kharaziha, A. Baidya, N. Annabi, Rational design of immunomodulatory hydrogels for chronic wound healing, Adv. Mater. 33 (39) (2021) e2100176.
[42] J. Park, J.S. Min, B. Kim, U.B. Chae, J.W. Yun, M.S. Choi, I.K. Kong, K.T. Chang, D. S. Lee, Mitochondrial ROS govern the LPS-induced pro-inflammatory response in microglia cells by regulating MAPK and NF-kappaB pathways, Neurosci. Lett. 584 (2015) 191–196.
[43] J. Tur, S. Pereira-Lopes, T. Vico, E.A. Marin, J.P. Munoz, M. Hernandez-Alvarez, P. J. Cardona, A. Zorzano, J. Lloberas, A. Celada, Mitofusin 2 in macrophages links mitochondrial ROS production, cytokine release, phagocytosis, autophagy, and bactericidal activity, Cell Rep. 32 (8) (2020) 108079.
[44] K. Khorsandi, R. Hosseinzadeh, H. Esfahani, K. Zandsalimi, F.K. Shahidi, H. Abrahamse, Accelerating skin regeneration and wound healing by controlled ROS from photodynamic treatment, Inflamm. Regen. 42 (1) (2022) 40.
[45] S.A. Eming, P. Martin, M. Tomic-Canic, Wound repair and regeneration: mechanisms, signaling, and translation, Sci. Transl. Med. 6 (265) (2014) 265sr6.
[46] S.P. Herbert, D.Y. Stainier, Molecular control of endothelial cell behaviour during blood vessel morphogenesis, Nat. Rev. Mol. Cell Biol. 12 (9) (2011) 551–564.
[47] H.S. Han, I. Jun, H.K. Seok, K.S. Lee, K. Lee, F. Witte, D. Mantovani, Y.C. Kim, S. Glyn-Jones, J.R. Edwards, Biodegradable magnesium alloys promote angio-osteogenesis to enhance bone repair, Adv. Sci. 7 (15) (2020) 2000800.
[48] N.A. Al Zahrani, R.M. El-Shishtawy, A.M. Asiri, Recent developments of gallic acid derivatives and their hybrids in medicinal chemistry: a review, Eur. J. Med. Chem. 204 (2020) 112609.
[49] A. Khatkar, A. Nanda, P. Kumar, B. Narasimhan, Synthesis, antimicrobial evaluation and QSAR studies of gallic acid derivatives, Arab. J. Chem. 10 (2017) S2870–S2880.
[50] J. Kang, L. Liu, M. Liu, X. Wu, J. Li, Antibacterial activity of gallic acid against Shigella flexneri and its effect on biofilm formation by repressing mdoH gene expression, Food Control 94 (2018) 147–154.
[51] Z. Zhou, S. Zhou, X. Zhang, S. Zeng, Y. Xu, W. Nie, Y. Zhou, T. Xu, P. Chen, Quaternary ammonium salts: insights into synthesis and new directions in antibacterial applications, Bioconjugate Chem. 34 (2) (2023) 302–325.
[52] L.A.T.W. Asri, M. Crismaru, S. Roest, Y. Chen, O. Ivashenko, P. Rudolf, J.C. Tiller, H.C. van der Mei, T.J.A. Loontjens, H.J. Busscher, A. Shape-Adaptive, Antibacterial-coating of immobilized quaternary-ammonium compounds tethered on hyperbranched polyurea and its mechanism of action, Adv. Funct. Mater. 24 (3) (2014) 346–355.
[53] L. Wang, M. Xin, M. Li, W. Liu, Y. Mao, Effect of the structure of chitosan quaternary phosphonium salt and chitosan quaternary ammonium salt on the antibacterial and antibiofilm activity, Int. J. Biol. Macromol. 242 (2023) 124877.
[54] R.S. Moreci, T. Lechler, Epidermal structure and differentiation, Curr. Biol. 30 (4) (2020) R144–R149.
[55] P.A. Coulombe, R. Kopan, E. Fuchs, Expression of keratin K14 in the epidermis and hair follicle: insights into complex programs of differentiation, J. Cell Biol. 109 (5) (1989) 2295–2312.
[56] R. Moll, W.W. Franke, D.L. Schiller, B. Geiger, R. Krepler, The catalog of human cytokeratins: patterns of expression in normal epithelia, tumors and cultured cells, Cell 31 (1) (1982) 11–24.
[57] V.L. Martins, M. Caley, E.A. O'Toole, Matrix metalloproteinases and epidermal wound repair, Cell Tissue Res. 351 (2) (2013) 255–268.
[58] B.N. Brown, R. Londono, S. Tottey, L. Zhang, K.A. Kukla, M.T. Wolf, K.A. Daly, J. E. Reing, S.F. Badylak, Macrophage phenotype as a predictor of constructive remodeling following the implantation of biologically derived surgical mesh materials, Acta Biomater. 8 (3) (2012) 978–987.
[59] Z.S. Gao, C.J. Zhang, N. Xia, H. Tian, D.Y. Li, J.Q. Lin, X.F. Mei, C. Wu, Berberine-loaded M2 macrophage-derived exosomes for spinal cord injury therapy, Acta Biomater. 126 (2021) 211–223.
[60] T.A. Wynn, K.M. Vannella, Macrophages in tissue repair, regeneration, and fibrosis, Immunity 44 (3) (2016) 450–462.
[61] C. Cheignon, M. Tomas, D. Bonnefont-Rousselot, P. Faller, C. Hureau, F. Collin, Oxidative stress and the amyloid beta peptide in Alzheimer's disease, Redox Biol. 14 (2018) 450–464.
[62] C.M. Sena, A. Leandro, L. Azul, R. Seica, G. Perry, Vascular oxidative stress: impact and therapeutic approaches, Front. Physiol. 9 (2018) 1668.
[63] C.T. Taylor, C.C. Scholz, The effect of HIF on metabolism and immunity, Nat. Rev. Nephrol. 18 (9) (2022) 573–587.
[64] S. Ramakrishnan, V. Anand, S. Roy, Vascular endothelial growth factor signaling in hypoxia and inflammation, J. Neuroimmune Pharmacol. 9 (2) (2014) 142–160.
[65] W. Liu, S. Guo, Z. Tang, X. Wei, P. Gao, N. Wang, X. Li, Z. Guo, Magnesium promotes bone formation and angiogenesis by enhancing MC3T3-E1 secretion of PDGF-BB, Biochem. Biophys. Res. Commun. 528 (4) (2020) 664–670.
[66] K. Funa, M. Sasahara, The roles of PDGF in development and during neurogenesis in the normal and diseased nervous system, J. Neuroimmune Pharmacol. 9 (2) (2014) 168–181.